Application of a Spectral Transform on Cubed-Sphere Grids to Representation of Forecast Errors for Variational Data Assimilation

Hyo-Jong Song[a], Jihye Kwun[b], and Sang-Yoon Jun[c]

[a] Data Assimilation Team, Korea Institute of Atmospheric Prediction Systems (KIAPS), Republic of Korea, hj.song@kiaps.org, [b] Data Assimilation Team, KIAPS, Republic of Korea, [c] Systems Development Team, KIAPS, Republic of Korea.

Motivations

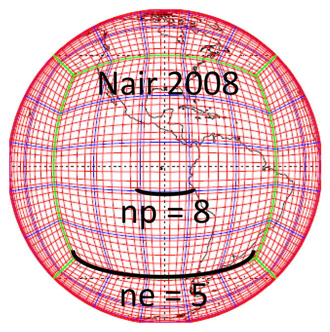

The spectral element (SE) method avoids the pole problem by using cubed-sphere grids in which the sphere is tiled with quadrilateral elements. The SE is ideal for its implementation on massive CPUs. While the communication within each element is global, elements need only boundary information from their neighboring elements. To date, application of the SE method to numerical atmospheric modeling has focused on climate prediction, e.g. CAM-SE. If we can develop data assimilation systems applicable to it, SE may be used for even NWP modeling.

Spectral transformations often have a role of horizontal filtering of error correlations in data assimilation systems. To apply Fourier and Legendre transformations for any fields given on cubed-sphere grids, we should have to interpolate the variables onto Gaussian grids. However, it yields interpolation errors and re-distribution of data on memories. We thus developed a spectral transformation method working directly on a cubed-sphere grid system.

Development of a Spectral Transformation on Cubed-Sphere Grids

A small displacement on a sphere (λ, θ, R) is defined as

$$d\mathbf{r} = R\cos\theta d\lambda\hat{\mathbf{e}}_\lambda + Rd\theta\hat{\mathbf{e}}_\theta \ .$$

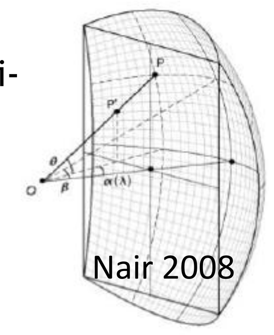

Unit vectors in an equi-angular coordinate (α, β, R) are non-orthogonal, that is, the equi-angular coordinate is a curvilinear system. (Nair 2008). The covariant unit vectors and covariant components are written as

$$\mathbf{a}_1 = \partial\mathbf{r}/\partial\alpha, \quad \mathbf{a}_2 = \partial\mathbf{r}/\partial\beta$$

$$v_1 = \mathbf{v}\cdot\mathbf{a}_1, \quad v_2 = \mathbf{v}\cdot\mathbf{a}_2$$

Then, a vector on the sphere can be expressed by contravariant components:

$$\mathbf{v} = v^1\mathbf{a}_1 + v^2\mathbf{a}_2.$$

A matrix (**D**) for transforming contravariant components in equi-angular coordinates to orthogonal components in spherical coordinate is

$$\mathbf{D} = (\mathbf{a}_1 \quad \mathbf{a}_2) = R\begin{pmatrix} \cos\theta\partial\lambda/\partial\alpha & \cos\theta\partial\lambda/\partial\beta \\ \partial\theta/\partial\alpha & \partial\theta/\partial\beta \end{pmatrix}$$

By using **D**, we can define a metric tensor g,

$$g_{ij} = \mathbf{a}_i\cdot\mathbf{a}_j = \mathbf{D}^{\mathrm{T}}\mathbf{D}$$

And the integration on the cubed-sphere grid is described as (Levy et al. 2008)

$$\boxed{\int_{-\pi/2}^{\pi/2}\int_0^{2\pi} f(\lambda,\theta)R^2 cos\theta d\lambda d\theta = \Sigma_k \int_{\Omega^k} f(\alpha,\beta)\sqrt{g}d\alpha d\beta}$$

In spherical coordinate, we obtain the spectral coefficients with the numerical integration of the following integrand:

$$f_l^m = \frac{1}{4\pi R^2}\int_{-\pi/2}^{\pi/2}\int_0^{2\pi} Y_l^m(\lambda,\theta)f(\lambda,\theta)R^2 cos\theta d\lambda d\theta$$

Here, Y_l^m is normalized spherical harmonic functions. It is in a real form

$$Y_l^m = \begin{cases} N_l^m P_l^m cos m\lambda(cos\theta) & \text{if } m > 0, \\ Y_l^0 & \text{if } m = 0, \\ N_l^{|m|} P_l^m sin|m|\lambda(cos\theta) & \text{if } m < 0. \end{cases}$$

With using the boxed formulation, in the cubed-sphere grid with equi-angular coordinates, the spectral transformation is

$$f_l^m = \frac{1}{4\pi R^2}\Sigma_k\int_{\Omega^k} Y_l^m(\alpha,\beta)f(\alpha,\beta)\sqrt{g}d\alpha d\beta$$

It is discretized as follows:

$$\boxed{f_l^m \approx \frac{1}{4\pi R^2}\Sigma_k(\Sigma_{i,j}\hat{Y}_{ij}\hat{f}_{ij}\sqrt{g_{ij}}w_i w_j)_k}$$

This is **the spectral transformation on the cubed-sphere grid with the equi-angular coordinates** (Song et al. 2013). w is the local Gaussian quadrature for each grid points in an element. A hat means the coefficients of Lagrange polynomials defined in each element:

$$f(\alpha,\beta) \approx \Sigma_{j=0}^N\Sigma_{i=0}^N\hat{f}_{ij}\phi_i(\alpha,\beta)\phi_j(\alpha,\beta)$$

Verification of the Spectral Transformation on Cubed-Sphere Grids

After 63 wavenumber, errors in orthogonality, eigenvalues of Laplacian defined in cubed-sphere grids, and synthesis abruptly increase wiith using ne = 16, np = 4 (Fig. 1).

When grid points should represent mo waves, accuracy of the estimation of the eigenvalues becomes less (Fig. 2).

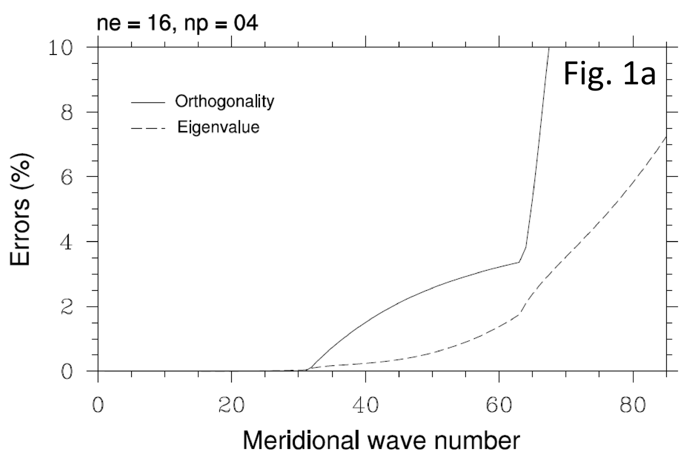

Fig. 1a

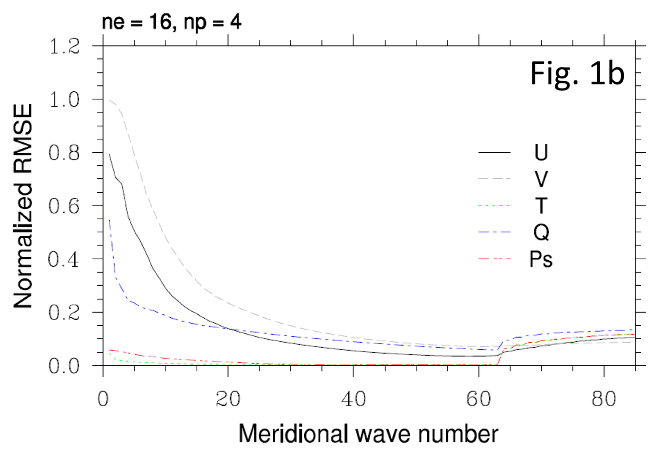

Fig. 1b

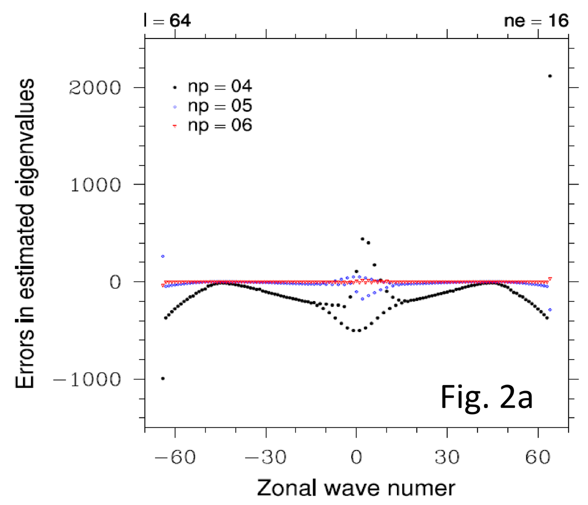

Fig. 2a

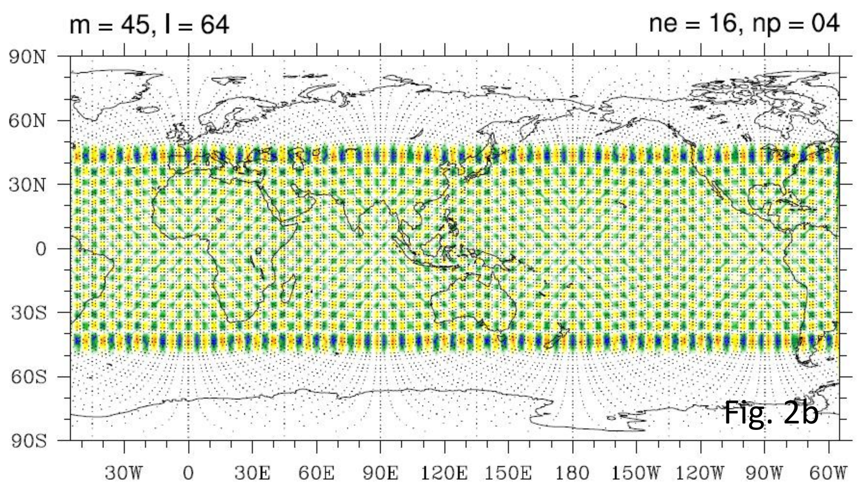

Fig. 2b

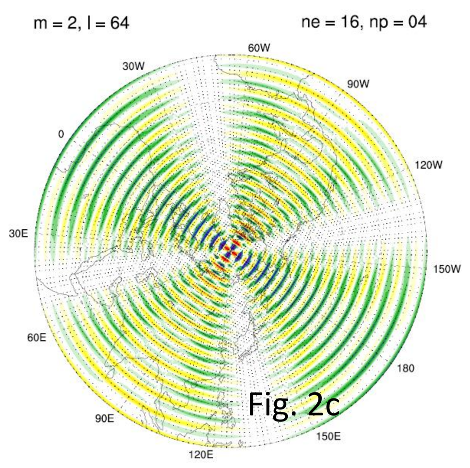

Fig. 2c

Application to Variational Data Assimilation

Climatological mean of March to June every 12 UTC after 2-year CAM-SE climatological run is used as a background state. Observations are radiosonde data on 12 UTC in 10 Aug. 2011 (the positions denoted by small dots in Fig. 5). A cost function of 3D-Var using the spectral transformation (**S**) and inverse is when **B**var means error variances for grid points

$$\delta\mathbf{v} = \mathbf{S}\sqrt{\mathbf{B}_{var}}^{-1}[\mathbf{x} - \mathbf{x}^b]$$

$$J(\delta\mathbf{v}) = \delta\mathbf{v}^{\mathrm{T}}\mathbf{B}_v^{-1}\delta\mathbf{v} + [\mathbf{y}^o - H(\mathbf{x}^b + \sqrt{\mathbf{B}_{var}}\mathbf{S}^{-1}\delta\mathbf{v})]^{\mathrm{T}}\mathbf{R}^{-1}[\mathbf{y}^o - H(\mathbf{x}^b + \sqrt{\mathbf{B}_{var}}\mathbf{S}^{-1}\delta\mathbf{v})]$$

$$\mathbf{x}^a = \mathbf{x}^b + \sqrt{\mathbf{B}_{var}}\mathbf{S}^{-1}\delta\mathbf{v}^a$$

The background error standard deviations of zonal winds have smaller scale in space than those of temperature do (Fig 3). To measure performance, we assume an ERA interim data corresponding to observation time as a truth. In Northern Hemisphere, the analysis increments of temperature well match the background error (Fig 4c,d and 5c,d). The analysis increments at 850 hPa in the Antarctic region against the background error is a interesting feature. In the case of zonal winds, on the NH continents having rich sondes, the analysis increments tend to reduce the background error. In Arctic regions, the phases of background errors and analysis increments are overlapped.

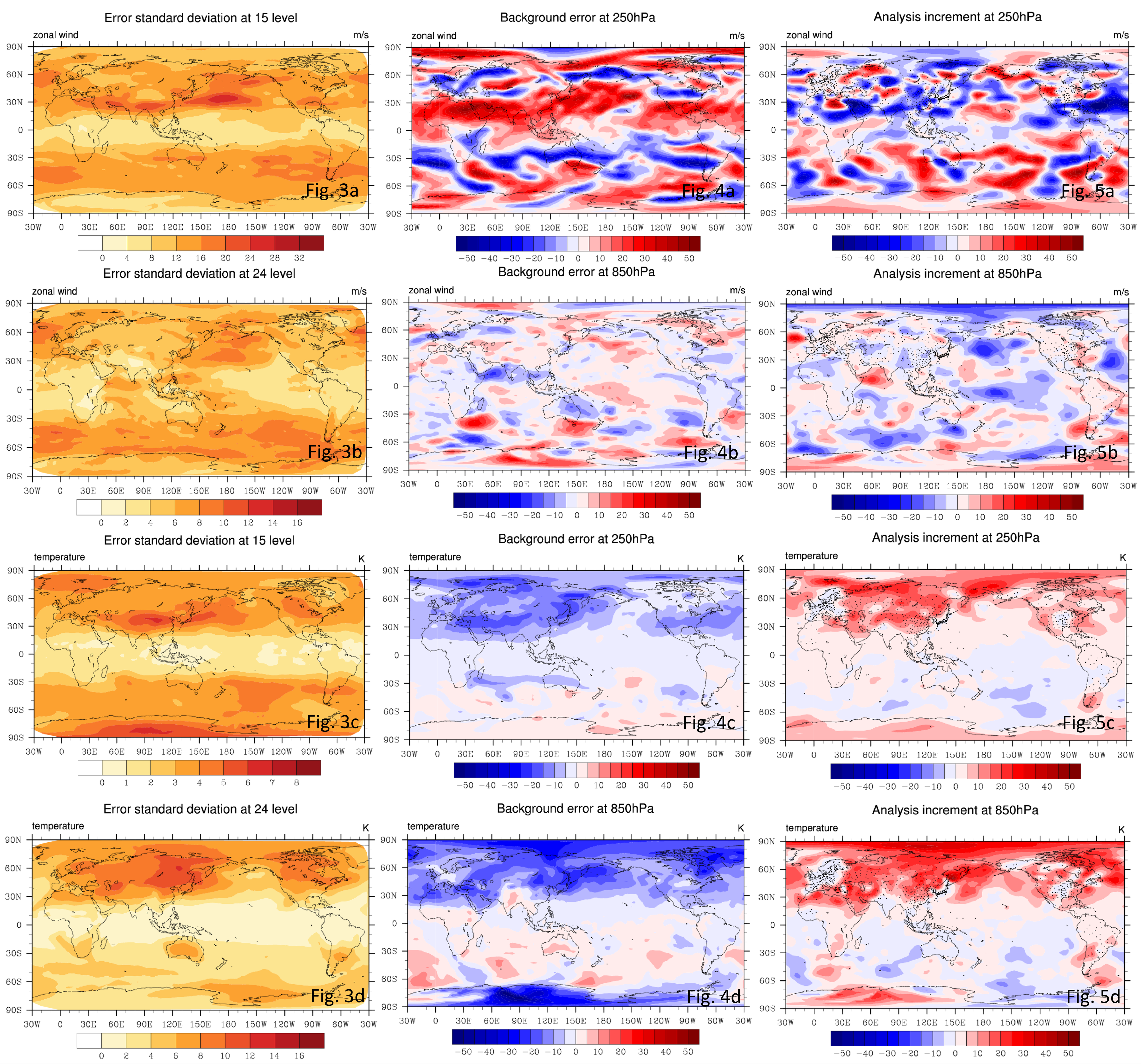

Fig. 3a Fig. 4a Fig. 5a Fig. 3b Fig. 4b Fig. 5b Fig. 3c Fig. 4c Fig. 5c Fig. 3d Fig. 4d Fig. 5d

Discussions

Analysis of zonal wind has large increments over the wavenumbers for baroclinic waves (Fig. 6a). The variance of deviations normalized by the error standard deviations on grids well show that the zonal wind have considerable amounts of variability around wavenumber 10 and it explains the feature of analysis increments (Fig. 6b). The substantial increments over high frequencies are considered as contributed by the error standard deviations having high-frequency feature (Fig 3a,b).

Temperature tends to have larger increments as wavenumber gets smaller (Fig. 6a). It is a reflection of the structure of the variance of the normalized deviations (Fig 6b). Note that even the grid-point error standard deviations of temperature have large-scale feature unlike those of zonal wind (Fig. 3).

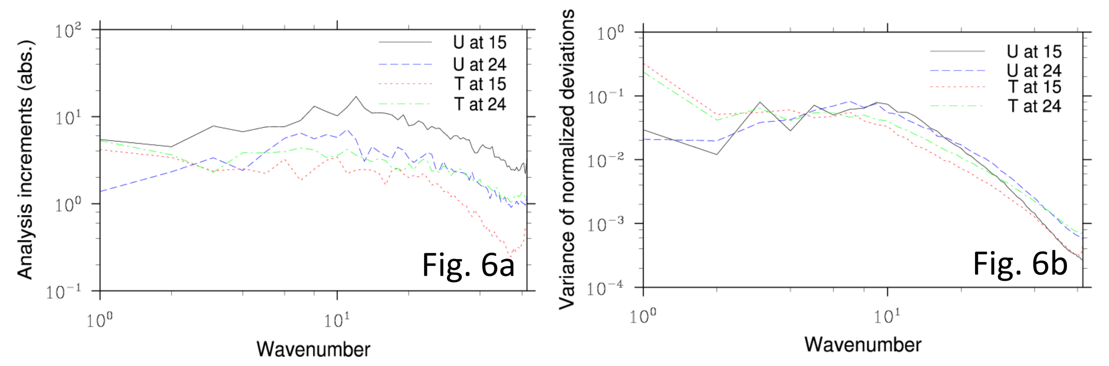

Fig. 6a Fig. 6b

Vertical error covariance for wavenumber 10 (zonal wavenumber 0) reveals baroclinic structure in zonal wind (variable index 1-30 corresponding to model level 1-30) (Fig. 7b). On the other hand, that for wavenumber 1 shows barotropic structures in zonal wind and temperature (variable index 31-60) (Fig. 7a). It supports the barotropic shape of analysis increment of temperature of which substantial portions are low-frequency components.

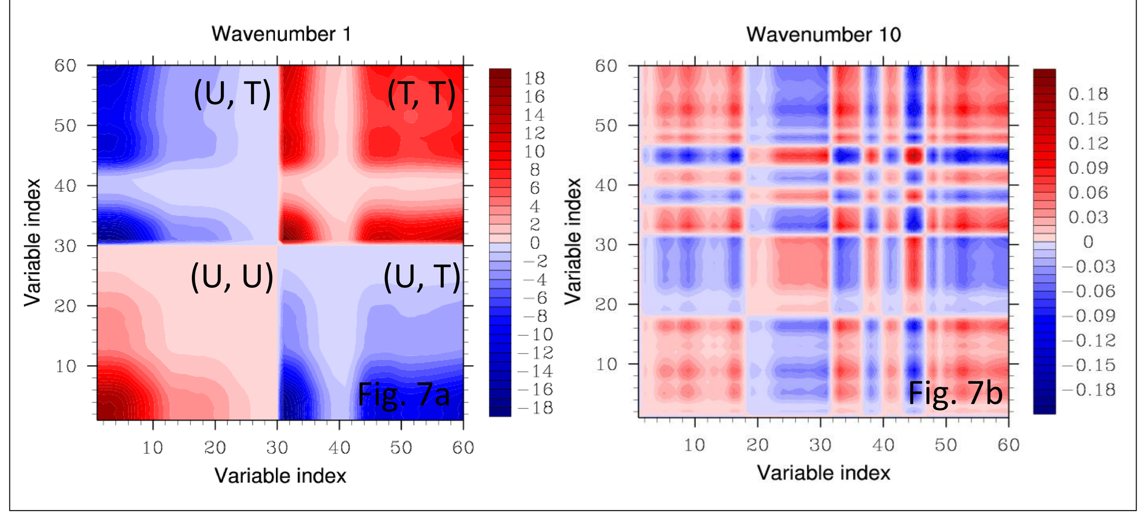

Fig. 7a Fig. 7b

Summary and Remarks

We developed spectral transformation modules that work on cubed-sphere grids. When the configuration of cubed-sphere grids is ne = 16, np = 4, we determined that the grid points can represent up to waves of wavenumber 63 (Fig. 1).

As a result of application to variational data assimilation, we obtain the understandable background error covariance structures and analysis increments (Fig. 3-7). The shapes of spectral error variance and vertical error covariance for two wavenumber coincide with climatological features of large-scale dynamics (Fig. 6 and 7).

Fig. 8 presents how each configuration of cubed-sphere grids can resolve the waves. The greater np is, the better the resolution of cubed-sphere grids is. Reproducing this experiment with a greater np and lower ne may be interesting.

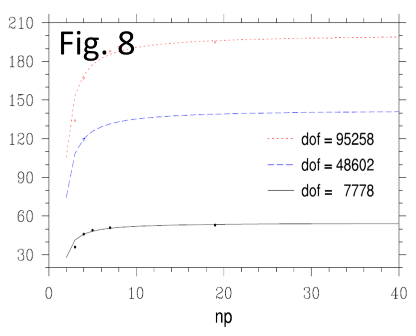

Fig. 8

References

Levy, M. N., R. D. Nair, and H. M. Tufo, 2008: A high-order element-based Galerkin method for the barotropic vorticity equation, *Int. J. Numer. Meth. Fluids*, DOI: 10.1002/fld.1874.

Nair, R., 2008: Cubed-sphere grids and Galerkin approaches, 2008 Global Atmospheric Core Workshop, September 23-24, Boulder CO, USA.

Song, H.-J., J. Kwun, and I.-S. Song, 2013: Development of spectral transforms on a cubed-sphere grid, 2013 Korean Meteorological Meeting, April 17-19, Seoul, Korea.

Acknowledgements

We are very thankful for Dr. Ji-Sun Kang's providing the results of CAM-SE run and Dr. Ha-Taek Kwon and Dr. Jeon-Ho Kang's supplying radiosonde data. Dr. In-Sun Song gave us valuable comments about the characteristics of spherical harmonics represented on the cubed-sphere grids.